A MATHEMATICAL MODEL FOR
FIBROBLAST GROWTH FACTOR COMPETITION
BASED ON ENZYME KINETICS

Justin P. Peters, Khalid Boushaba

Department of Mathematics, Iowa State University
Carver Hall, Ames, IA 50011

Marit Nilsen-Hamilton

Department of Biochemistry, Biophysics, and Molecular Biology,
Iowa State University, Biology Building Ames, IA 50011

(Communicated by Howard A. Levine)

Abstract. In this paper, we develop a mathematical model for the competition of two species of fibroblast growth factor, FGF-1 and FGF-2, for the same cell surface receptor. We provide pathways for this interaction using experimental data obtained by Neufeld and Gospodarowicz reported in 1986 [9]. These pathways demonstrate how the interaction of two fibroblast growth factors affects cell proliferation. Upon development of these pathways, we use simulations in MATLAB and optimization to extrapolate the values of a variety of biochemical parameters imbedded within the model. Furthermore, it should be possible to use the model as the basis for a testable hypothesis. We explore this predictive ability with further simulations in MATLAB.

1. **Introduction.** Fibroblast growth factors (FGFs), among the earliest growth factors to be identified and purified, constitute a large family of at least 25 unique but related secreted proteins that stimulate cell proliferation and that are expressed in many tissues. The levels of FGFs found in these tissues are regulated by many biological factors, which reflects the involvement of the FGFs in more than one physiological event. One important physiological function of FGFs is in wound healing. The role of FGFs in wound healing has been demonstrated in many ways, among them FGFs are found in wound fluids, the absence of FGF2 delays wound healing [6], and the expression of many FGF genes increases after wounding [8]. In combination with other growth factors, FGFs also play many roles in early embryonic development including to define the dorso-ventral pattern of the neural tube [14], to promote limb development [11], and to define the structure of the early embryo [3]. The FGFs act through specific receptors (FGFR) that initiate signals inside the cell to alter cellular functions such as gene expression. The importance of these receptors to normal development is demonstrated by the many human skeletal diseases caused by mutations in FGFR genes [15].

Four related FGFR genes are the source of 12 different FGF receptor proteins. Each receptor protein binds more than one FGF type, each with a specific affinity that is determined by the receptor-FGF pair. Many studies have shown that more than one FGF is produced in a tissue at the same time. For example, in the skin the genes encoding FGFs 1, 2, 3, 5, 6, 7, 9, 10, 11, 12, 13, 16, 18, 20, 22, and 23 are simultaneously active during wound healing. Thus, in vivo, FGF receptors are exposed to more than one FGF at simultaneously. In most cases the cellular response is determined by the nature of the receptor and not by the ligand (FGF), although there are some possible exceptions [5]. However, the response of the receptor depends on the interplay of FGFs present in the environment and their affinities for the receptor. Here we examine a simple case of two FGFs (FGF-1 and FGF-2) interacting with the receptors on a single cell type in cultured cells. Using the biological data, we develop a mathematical model that simulates the competition between these growth factors for the same cell surface receptors . The construct of the first pathway of this model looks similar to that of [2] in that the basis for the model is a system of coupled differential equations; however, the underlying mechanism being modeled is different. In [2], the authors examine the effects of FGF-2 and an inhibitor of growth of both primary and secondary tumors; whereas, this study aims to model how the interaction of two fibroblast growth factors affects cell proliferation. The construct for the remaining pathways of the model differs in that these pathways yield a model without differential equations. After deriving the model for each of the pathways in [9], we use simulations in MATLAB and optimization to extrapolate the values of a variety of biochemical parameters imbedded within the model. Finally, we examine use of the model as the basis for a testable hypothesis. We explore this predictive ability with further simulations in MATLAB.

2. **Biological Activity of FGF-1 and FGF-2.** In [9], Neufeld and Gospodarowicz examined the physical and chemical characteristics of FGF-1 and FGF-2.[1] Noting the apparent similarities between FGF-1 and FGF-2, Neufeld and Gospodarowicz proceeded to investigate the differential affinities of these two FGFs to the same cell surface receptor. Several experiments were carried out to characterize biological activity of FGF-1 and FGF-2 in a variety of different situations.

Experiment 1. First, the effects of increasing concentrations of either FGF-1 and FGF-2 on cell proliferation were observed. Neufeld and Gospodarowicz began with plates each containing 4×10^4 cells from a baby hamster kidney cell line (BHK-21). One set of plates was exposed to increasing concentrations of FGF-1 (ranging from 50 pg/mL to 250 ng/mL), while another set of plates was exposed to increasing concentrations of FGF-2 (ranging from 2.5 pg/mL to 25 ng/mL). These increments of growth factor were added in two boluses, one on day 0 and one on day 2. After 4 days, the number of cells on each plate was counted and recorded. These data were displayed as FIG 2 in [9], recreated here as Figure 1.

Experiment 2. Next, Neufeld and Gospodarowicz examined the ability of FGF-1 and FGF-2 to displace iodinated forms of both FGFs. This experiment functioned as a test to determine if FGF-1 could compete with FGF-2 the same cell surface

---

[1]At the time [9] was in publication, FGF-1 and FGF-2 were referred to as acidic and basic fibroblast growth factor, respectively. For comprehensibility we will continue to employ the numerical notation to refer to these FGFs.
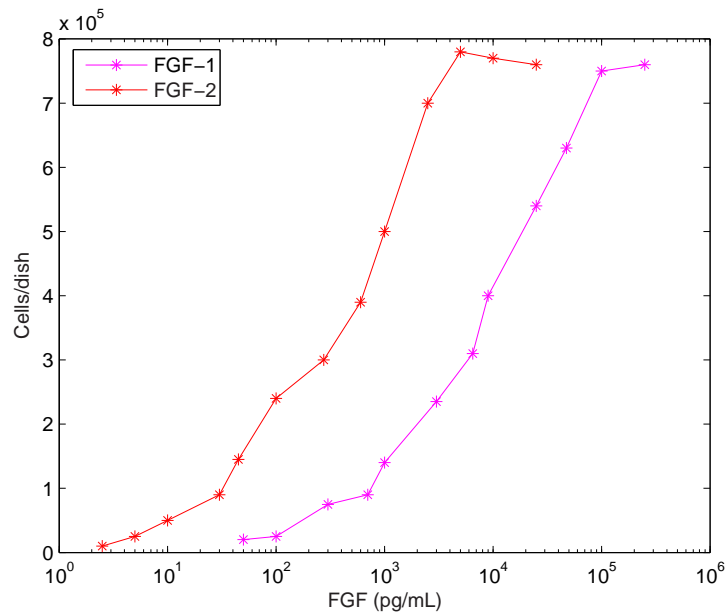
FIGURE 1. Effects of FGF-1 and FGF-2 Concentration on Proliferation of BHK-21 Cells (from [9])

receptor. In these experiments, the growth factors were labeled with [125]I. Then BHK-21 cell membranes were incubated for 30 minutes in the presence of either ^{125}I-FGF-1 (13 ng/mL) or ^{125}I-FGF-2 (14 ng/mL) and in the absence of competing unlabeled FGF. These values represented the maximal amount of ^{125}I-FGF-1 and ^{125}I-FGF-2 binding, respectively. Next, increasing concentrations of unlabelled FGF-1 and FGF-2 were added to 13 ng/mL ^{125}I-FGF-1 and then separately added to 14 ng/mL ^{125}I-FGF-2. Iodinated FGF binding was recorded and appeared in parts B and A, respectively, in figure 4 from [9], recreated here as Figure 2.[2]

Figures 1 and 2 serve as the standard against which we reference the fit of the models during development. We now begin formulation of the models by examining the biochemical kinetics involved in the competitive pathways of each experiment.

3. Biochemical Kinetics.

3.1. **Experiment 1.** The first competitive pathway is as follows: Suppose R is a free receptor on a BHK-21 cell capable of being activated by either FGF-1 or FGF-2. Let G^1 be a molecule of FGF-1. Then, the binding of FGF-1 to a free receptor leads to an intermediate complex, $\{RG^1\}$, which releases a product, call it P^1, by the mechanism:

$$R + G^1 \underset{k_{-1}}{\overset{k_1}{\rightleftharpoons}} \{RG^1\},$$

$$\{RG^1\} \overset{k_2}{\rightarrow} P^1. \tag{1}$$
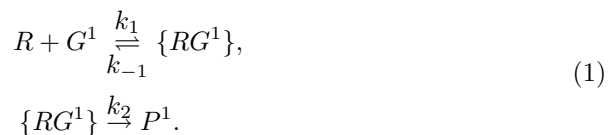
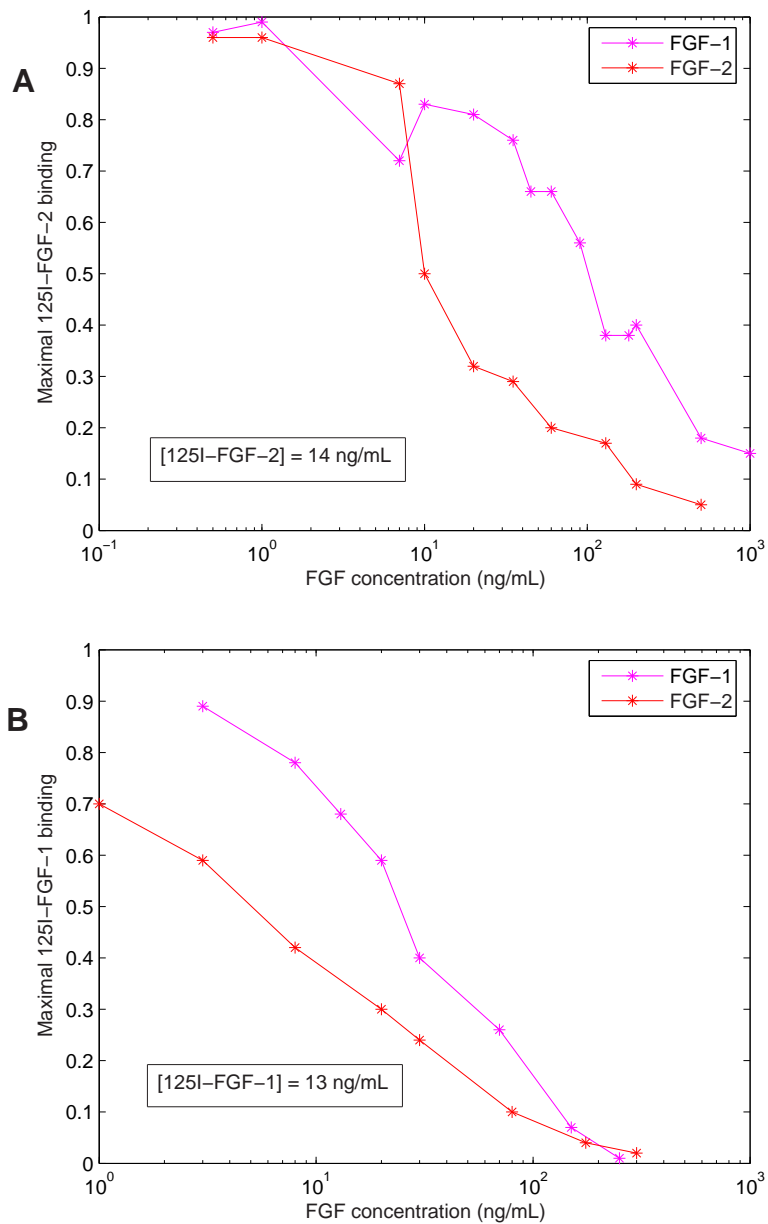[2]The points appearing at (0,1) in [9] are omitted here because of the distortion they would produce on the x-axes.

FIGURE 2. Competitive Inhibition in the Binding of ^{125}I-FGF-1 and ^{125}I-FGF-2 to BHK-21 Cell Membranes by Unlabelled FGF-1 and Unlabelled FGF-2 (from [9])

The product P^1 begins a tyrosine-kinase signal transduction pathway leading to an increase in cell number.[3] Concurrently occurring is the binding of FGF-2, G^2,

_____

[3]The exact pathway leading to increased cell proliferation is long and involved. For the present discussion, it suffices that the intermediate complex begins a signal transduction pathway ultimately resulting in increased proliferation; hence, this simplification is used for the present model.

to another free receptor, R. This binding also leads to an intermediate complex, $\{RG^2\}$, which again releases a product, P^2:

$$R + G^2 \underset{k_{-3}}{\overset{k_3}{\rightleftharpoons}} \{RG^2\},$$

$$\{RG^2\} \overset{k_4}{\rightarrow} P^2. \tag{2}$$
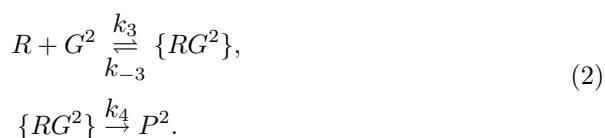
Product P^2 also initiates a signal transduction pathway. This cascade again results in increased cell numbers. When both species of growth factor are present, the interplay of these two equations, (1) and (2), results in competition of both species for the same free receptors:
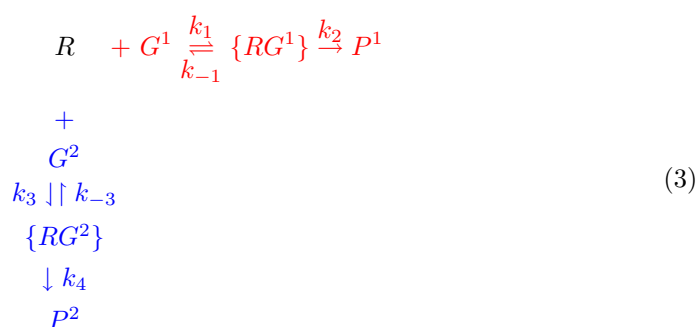
$$
\begin{array}{c}
R \quad + G^1 \underset{k_{-1}}{\overset{k_1}{\rightleftharpoons}} \{RG^1\} \overset{k_2}{\rightarrow} P^1 \\[1em]
+ \\
G^2 \\
k_3 \downarrow\uparrow k_{-3} \\
\{RG^2\} \\
\downarrow k_4 \\
P^2
\end{array}
\tag{3}
$$

Table 1 summarizes the species present in this pathway.

TABLE 1. **Notation for Species in Kinetic Equations**

Species	Notation
free receptor	R
fibroblast growth factor, FGF-1	G^1
fibroblast growth factor, FGF-2	G^2
product initiating cell proliferation	P^1
product initiating cell proliferation	P^2

This competitive pathway is further developed by writing down the laws of mass action[4] for (1) and (2), as follows[5] [6]:

$$\frac{d[G^1]}{dt} = k_{-1}[\{RG^1\}] - k_1[R][G^1],$$
$$\frac{d[\{RG^1\}]}{dt} = -(k_{-1} + k_2)[\{RG^1\}] + k_1[R][G^1],$$
$$\frac{d[G^2]}{dt} = k_{-3}[\{RG^2\}] - k_3[R][G^2],$$
$$\frac{d[\{RG^2\}]}{dt} = -(k_{-3} + k_4)[\{RG^2\}] + k_3[R][G^2]$$

(4)

At this point we employ the Michaelis-Menten steady-state assumption explained in [13]. Essentially, this assumption states that following the initial stage of the reaction, termed the transient phase, the rate of synthesis of an intermediate remains approximately equal to the rate of consumption of said intermediate until the substrate, or growth factor in the present example, is nearly exhausted. Thus, a quasi-equilibrium is reached. Applying this hypothesis, we take the concentrations of both intermediates to be constant, and using the notation $K_M^i = (k_{2i} + k_{-(2i-1)})/k_{2i-1}$

---

[4]In this paper, we employ the chemical convention whereby [A] denotes the local concentration of species A in micromoles per liter, or micromolarity.

[5]It is important to remark that the first and third equations in (4) have been simplified. Taking into account cell expression and FGF turnover rate, these equations are more completely written as:

$$\frac{d[G^1]}{dt} = k_{-1}[\{RG^1\}] - k_1[R][G^1] + \sigma_{G^1}[R]_T - \mu_{G^1}[G^1],$$
$$\frac{d[G^2]}{dt} = k_{-3}[\{RG^2\}] - k_3[R][G^2] + \sigma_{G^2}[R]_T - \mu_{G^2}[G^2],$$

where σ_{G^1} and σ_{G^2} are constants for cellular expression of G^1 and G^2, respectively, and μ_{G^1} and μ_{G^2} are decay rates for the aforementioned growth factors, and $[R]_T$ is the total concentration of receptors. We may neglect σ_{G^1} and σ_{G^2} because the expression of either growth factor by the BHK-21 cells is negligible relative to the concentration of growth factor being added into the cell cultures. Likewise, we may neglect μ_{G^1} and μ_{G^2} because the decay rate of either growth factor is negligible relative to the concentration of growth factor being consumed by the growing cell populations. Essentially, FGF-1 and FGF-2 are being consumed by the cells at a far faster rate than either half-life would allow for decay.

[6]It is important to remark that the first and third equations in (4) have been simplified. Taking into account cell expression and FGF turnover rate, these equations are more completely written as:

$$\frac{d[G^1]}{dt} = k_{-1}[\{RG^1\}] - k_1[R][G^1] + \sigma_{G^1}[R]_T - \mu_{G^1}[G^1],$$
$$\frac{d[G^2]}{dt} = k_{-3}[\{RG^2\}] - k_3[R][G^2] + \sigma_{G^2}[R]_T - \mu_{G^2}[G^2],$$

where σ_{G^1} and σ_{G^2} are constants for cellular expression of G^1 and G^2, respectively, and μ_{G^1} and μ_{G^2} are decay rates for the aforementioned growth factors, and $[R]_T$ is the total concentration of receptors. We may neglect σ_{G^1} and σ_{G^2} because the expression of either growth factor by the BHK-21 cells is negligible relative to the concentration of growth factor being added into the cell cultures. Likewise, we may neglect μ_{G^1} and μ_{G^2} because the decay rate of either growth factor is negligible relative to the concentration of growth factor being consumed by the growing cell populations. Essentially, FGF-1 and FGF-2 are being consumed by the cells at a far faster rate than either half-life would allow for decay.

for each Michaelis constant, the second and fourth equations in (4) become:

$$[\{RG^1\}] = \frac{[R][G^1]}{K_M^1},$$
$$[\{RG^2\}] = \frac{[R][G^2]}{K_M^2}. \tag{5}$$

Substituting the first and second equations of (5) into the first and third equations of (4), respectively, yields:

$$\frac{d[G^1]}{dt} = k_{-1}K_M^1[R][G^1] - k_1[R][G^1] = -\frac{k_2}{K_M^1}[R][G^1],$$
$$\frac{d[G^2]}{dt} = k_{-3}K_M^2[R][G^2] - k_3[R][G^2] = -\frac{k_4}{K_M^2}[R][G^2]. \tag{6}$$

Next, we relate cell density to receptor concentration. We assume, as noted in [2], that the number of BHK-21 cells per unit volume is proportional to the total number of receptors that can initiate a signal transduction pathway in response to a growth factor. Thus, we may write

$$[N] = \kappa[R]_T, \tag{7}$$

where [N] denotes the concentration of BHK-21 cells, $[R]_T$ denotes the total concentration of receptors, and κ is the proportionality constant. Substituting R_0/N_0 for the proportionality constant κ, we may write:

$$[R]_T = R_0 \frac{[N]}{N_0}, \tag{8}$$

where N_0 is the carrying capacity of the BHK-21 cells and R_0 is the total number of receptors at carrying capacity. As [2] explains, we may take R_0 to be on the order of unity; thus, our relationship becomes:

$$[R]_T = \frac{[N]}{N_0}. \tag{9}$$

Furthermore, we may write the total concentration of receptors as follows:

$$[R]_T = [R] + [\{RG^1\}] + [\{RG^2\}]. \tag{10}$$

Substituting the first and second equations of (5) into (10) yields:

$$[R]_T = [R] + \frac{[R][G^1]}{K_M^1} + \frac{[R][G^2]}{K_M^2}. \tag{11}$$

Solving for free receptors, $[R]$, gives

$$[R] = \frac{[R]_T}{1 + \frac{[G^1]}{K_M^1} + \frac{[G^2]}{K_M^2}}. \tag{12}$$

Substitution of (8) into (12) yields:

$$[R] = \frac{\frac{[N]}{N_0}}{1 + \frac{[G^1]}{K_M^1} + \frac{[G^2]}{K_M^2}}. \tag{13}$$

Finally, (13) can be substituted into the first and second equations of (6), as follows:

$$\frac{d[G^1]}{dt} = \left(\frac{-k_2\frac{[G^1]}{K_M^1}}{1 + \frac{[G^1]}{K_M^1} + \frac{[G^2]}{K_M^2}}\right)\frac{[N]}{N_0},$$

$$\frac{d[G^2]}{dt} = \left(\frac{-k_4\frac{[G^2]}{K_M^2}}{1 + \frac{[G^1]}{K_M^1} + \frac{[G^2]}{K_M^2}}\right)\frac{[N]}{N_0}.$$

$$(14)$$

Describing cell proliferation is slightly more complex but accomplished when several biological considerations are taken into account. First, we assume that cell proliferation is logistic as determined from the characteristic shape of Figure 1. Secondly, as noted in [2], it is reasonable to assume that BHK-21 cell mitosis depends on the concentrations of both growth factors and BHK-21 cell apoptosis is linear in cell density. These considerations allow us to write:

$$\frac{d[N]}{dt} = \phi(G^1, G^2)[N]\left(1 - \frac{[N]}{N_0}\right) - \mu[N], \tag{15}$$

where $\phi(G^1, G^2)$ is the coefficient of the logistic term and μ is the decay rate of BHK-21 cells. The term $\phi(G^1, G^2)$ is a measure of how the growth factors influence mitosis. In the present model, $\phi(G^1, G^2)$ takes the form:

$$\phi(G^1, G^2) = \lambda\left(\frac{\frac{[G^1]}{K_M^1} + \frac{[G^2]}{K_M^2}}{1 + \frac{[G^1]}{K_M^1} + \frac{[G^2]}{K_M^2}}\right). \tag{16}$$

As explained in [2], the underlying idea is that sufficient concentrations of either growth factor are necessary for the birth rate to exceed the death rate, but the effects of FGF-1 and FGF-2 on birth rate at saturation of either growth factor are limited to a maximum value of λ. Thus, the equation for cell proliferation becomes:

$$\frac{d[N]}{dt} = \lambda[N]\left(1 - \frac{[N]}{N_0}\right)\left(\frac{\frac{[G^1]}{K_M^1} + \frac{[G^2]}{K_M^2}}{1 + \frac{[G^1]}{K_M^1} + \frac{[G^2]}{K_M^2}}\right) - \mu[N]. \tag{17}$$

Combining this equation with the equations in (14), we obtain our first model, a system of three partial differential equations:

$$\frac{d[N]}{dt} = \lambda[N]\left(1 - \frac{[N]}{N_0}\right)\left(\frac{\dfrac{[G^1]}{K_M^1} + \dfrac{[G^2]}{K_M^2}}{1 + \dfrac{[G^1]}{K_M^1} + \dfrac{[G^2]}{K_M^2}}\right) - \mu[N],$$

$$\frac{d[G^1]}{dt} = \left(\frac{-k_2\dfrac{[G^1]}{K_M^1}}{1 + \dfrac{[G^1]}{K_M^1} + \dfrac{[G^2]}{K_M^2}}\right)\frac{[N]}{N_0}, \tag{18}$$

$$\frac{d[G^2]}{dt} = \left(\frac{-k_4\dfrac{[G^2]}{K_M^2}}{1 + \dfrac{[G^1]}{K_M^1} + \dfrac{[G^2]}{K_M^2}}\right)\frac{[N]}{N_0}.$$

3.2. **Experiment 2.** Next we explore the competition of unlabelled FGF with iodinated FGF. The first competitive pathway of Experiment 2 is much the same as the pathway for Experiment 1 in that a free receptor, R, on a BHK-21 cell is capable of being activated by either of two species; however, in this pathway, the species are FGF-1 and iodinated FGF-2. Suppose as earlier G^1 is a molecule of FGF-1, and let G^{2*} be a molecule of iodinated FGF-2. Then, the binding of FGF-1 to a free receptor leads to an intermediate complex, $\{RG^1\}$, by the equilibrium:

$$R + G^1 \underset{k_{-1}}{\overset{k_1}{\rightleftharpoons}} \{RG^1\}. \tag{19}$$

Again, there is competition for the free receptors; however, this time the competing species is iodinated FGF-2. The binding of iodinated FGF-2 to a free receptor also leads to the formation of the intermediate complex, $\{RG^{2*}\}$, by the equilibrium[7]:

$$R + G^{2*} \underset{k_{-3}}{\overset{k_3}{\rightleftharpoons}} \{RG^{2*}\}. \tag{20}$$

In a similar fashion we may write chemical equations for each of the remaining three pathways. Table 2 summarizes the species present in these pathways.

TABLE 2. **Notation for Additional Species in Kinetic Equations**

Species	Notation
fibroblast growth factor, FGF-1	G^1
fibroblast growth factor, FGF-2	G^2
iodinated FGF-1	G^{1*}
iodinated FGF-2	G^{2*}

[7]It is important to remark that the rate constants used in chemical equations (19) and (20) are equivalent to the respective rate constants used in the previous model. Even though we are currently constructing a pathway that involves iodinated FGF-2, we assume that it behaves biochemically the same as unlabelled FGF-2 and consequently displays the same reaction rate. This principle holds true for all subsequent repetitions of rate constants.

We may write the dissociation expression for chemical equation (20) in terms of the intermediate, as follows:

$$[\{RG^{2*}\}] = \frac{[R][G^{2*}]}{K_D^2}, \tag{21}$$

where the dissociation constant K_D^2 is given by $K_D^i = k_{-(2i-1)}/k_{2i-1}$. The astute reader will notice that equation (21) takes the same form as the equations in (5), where now we are dealing with dissociation constants rather than Michaelis constants. Nevertheless, we may make a substitution for free receptors similar to that of equation (12) in experiment 1 to obtain a model for the first pathway in experiment 2, as follows:

$$[\{RG^{2*}\}] = \frac{[R]_T \dfrac{[G^{2*}]}{K_D^2}}{1 + \dfrac{[G^1]}{K_D^1} + \dfrac{[G^{2*}]}{K_D^2}} = \frac{[R]_T[G^{2*}]}{K_D^2 + \dfrac{K_D^2}{K_D^1}[G^1] + [G^{2*}]}. \tag{22}$$

Using similar methods we obtain the models for each pathway in experiment 2. A summary of these four pathways is shown below:

$$[\{RG^{2*}\}] = \frac{[R]_T[G^{2*}]}{K_D^2 + \dfrac{K_D^2}{K_D^1}[G^1] + [G^{2*}]},$$

$$[\{RG^{2*}\}] = \frac{[R]_T[G^{2*}]}{K_D^2 + [G^2] + [G^{2*}]},$$

$$[\{RG^{1*}\}] = \frac{[R]_T[G^{1*}]}{K_D^1 + [G^1] + [G^{1*}]},$$

$$[\{RG^{1*}\}] = \frac{[R]_T[G^{1*}]}{K_D^1 + \dfrac{K_D^1}{K_D^2}[G^2] + [G^{1*}]}. \tag{23}$$

It is important to remark that the design of experiment 2, as carried out in [9], does not depend on the initial concentration of iodinated FGF nor the value of $[R]_T$, because the final concentration of iodinated FGF is plotted as a fraction of the maximum. To understand this observation more fully, we examine the parameter $[R]_T$. We see from (22) that the concentration of ^{125}I-FGF-2 depends on $[G^1]$, $[G^{2*}]$, K_D^1, and K_D^2. Furthermore, we note that only the value of $[G^1]$ changes and thus $[\{RG^{2*}\}]$ varies only with changes in $[G^1]$. Now we consider the normalization of $[\{RG^{2*}\}]$. Each entry of $[\{RG^{2*}\}]$ is divided by the first entry, the maximum, to yield a fraction of the total binding. Thus, we may write (22) as follows:

$$[\{RG^{2*}\}]_i = \frac{\dfrac{[R]_T[G^{2*}]}{K_D^2 + \dfrac{K_D^2}{K_D^1}[G^1]_i + [G^{2*}]}}{\dfrac{[R]_T[G^{2*}]}{K_D^2 + \dfrac{K_D^2}{K_D^1}[G^1]_1 + [G^{2*}]}}, \tag{24}$$

where $[A]_i$ represents the concentration of species A at each data point i. Here we see that, not only is the plot of $[\{RG^{2*}\}]$ independent of the initial concentration of

iodinated FGF, it is also independent of $[R]_T$ and the entire numerator, including $[G^{2*}]$, for we may simplify (24) to yield

$$[\{RG^{2*}\}]_i = \frac{K_D^2 + \dfrac{K_D^2}{K_D^1}[G^1]_i + [G^{2*}]}{K_D^2 + \dfrac{K_D^2}{K_D^1}[G^1]_1 + [G^{2*}]}. \tag{25}$$

Hence, we rewrite the equations in (23), taking into account these observations of normalization, as follows:

$$
\begin{aligned}
[\{RG^{2*}\}] &= K_D^2 + \frac{K_D^2}{K_D^1}[G^1] + [G^{2*}], \\
[\{RG^{2*}\}] &= K_D^2 + [G^2] + [G^{2*}], \\
[\{RG^{1*}\}] &= K_D^1 + [G^1] + [G^{1*}], \\
[\{RG^{1*}\}] &= K_D^1 + \frac{K_D^1}{K_D^2}[G^2] + [G^{1*}].
\end{aligned}
\tag{26}
$$

4. **Simulations and Optimization.** Now that we have constructed a model for each of the competitive pathways, we use MATLAB to simulate the experiments performed by Neufeld and Gospodarowicz in [9].

4.1. **Experiment 1.** For the pathway involving differential equations, we use the MATLAB solver ODE15s for simulations. First, we simulate the initial trial performed by Neufeld and Gospodarowicz in [9]. In this trial, cell plates containing 4×10^4 BHK-21 cells were exposed to increasing concentrations of FGF-1 in the absence of FGF-2. The added amounts of FGF-1 are shown in the first column of Table 3.

TABLE 3. **Concentrations of FGF-1 and FGF-2 for Experiment 1: (Added Day 0 and Day 2)**

FGF-1 concentration (no FGF-2 present)	FGF-2 concentration (no FGF-1 present)
50 pg/mL	2.5 pg/mL
100 pg/mL	5 pg/mL
300 pg/mL	10 pg/mL
700 pg/mL	30 pg/mL
1 ng/mL	45 pg/mL
3 ng/mL	100 pg/mL
6.5 ng/mL	275 pg/mL
9 ng/mL	600 pg/mL
25 ng/mL	1 ng/mL
47.5 ng/mL	2.5 ng/mL
100 ng/mL	5 ng/mL
250 ng/mL	10 ng/mL
	25 ng/mL

Thus, the initial conditions for our model are $[N] = 4 \times 10^4$, $[G^1]$ = column 1 of Table 3, and $[G^2] = 0$. Furthermore, $[G^2] = 0$ for the equations in (18) because no FGF-2 is present. This observation means that in this particular trial, the model

does not depend on the values of k_4 and K_M^2 from the second equation of (18). However, the model does require values for the parameters μ, λ, N_0, k_2, and K_M^1. These values were approximated in [2] and are shown in Table 4.

TABLE 4. **Numerical Values of Parameters Used in Simulations**

Parameter	Numerical Value (from [2])
μ	1.0×10^{-2} h^{-1}
λ	6.4×10^{-1} h^{-1}
N_0	775,000 cells
k_2	1.7 h^{-1}
K_M^1	1.83×10^{-2} μM
k_4	1×10^{-1} h^{-1}
K_M^2	1.19×10^{-2} μM

We now use the ODE15s solver to find the concentration of FGF-1 at time 48 hours.[8] To this concentration of FGF-1 we add the second bolus of growth factor, again expressed in column 1 of Table 3. Finally, we use the solver to determine the number of BHK-21 cells at time 72 hours.

Using a similar method, we simulate increasing concentrations of FGF-2. In this trial there is no FGF-1 present, (i.e. $[G^1] = 0$), and the model does not depend on the values of k_2 and K_M^1 from the equations in (18). Instead, this model utilizes the parameters μ, λ, N_0, k_4, and K_M^2. Numerical values for these parameters were again supplied by [2] and are given in Table 4. Again, by solving the system of differential equations twice, employing the pulse of additional growth factor described earlier, we obtain an approximation of the biological data. The data for both trials are plotted along with the associated biological data from Figure 1 in Figure 3.[9]

We now employ optimization to extrapolate the numerical values of the parameters appearing in the model. In the first trial of this experiment, these parameters are μ, λ, N_0, k_2, and K_M^1. To find the values of these parameters, which give the closest fit to the actual biological data, we first define an error function. This function is the sum of the squares of the differences of the biological data for cell density and the data calculated from the model for cell density, as represented below:

$$E = \sum_{i=1}^{n} (N_i^{\mathrm{exp}} - N_i^{\mathrm{model}})^2. \tag{27}$$

This error function has the values of the parameters as inputs. Different values for the parameters yield a different numerical value for the error function. Then, using a tool in MATLAB known as fminsearch, we minimize the error function and the resultant output is a vector of the values of the parameters which give the closest fit to actual biological data. Using fminsearch for the first trial, the resulting coefficient vector is:

$$\begin{bmatrix} 0.014162 & 0.468937 & 790,568 & 1.952589 & 0.012074 \end{bmatrix},$$

which corresponds to the values for μ, λ, N_0, k_2, and K_M^1. Likewise, we apply an error function to the second trial. Here, we are searching for the values of the

---

[8]This simulation uses hours for the time scale, as opposed to days in [9].

[9]As a convention for this paper, all biological data appear in shades of red; whereas, all data from models appear in shades of blue.
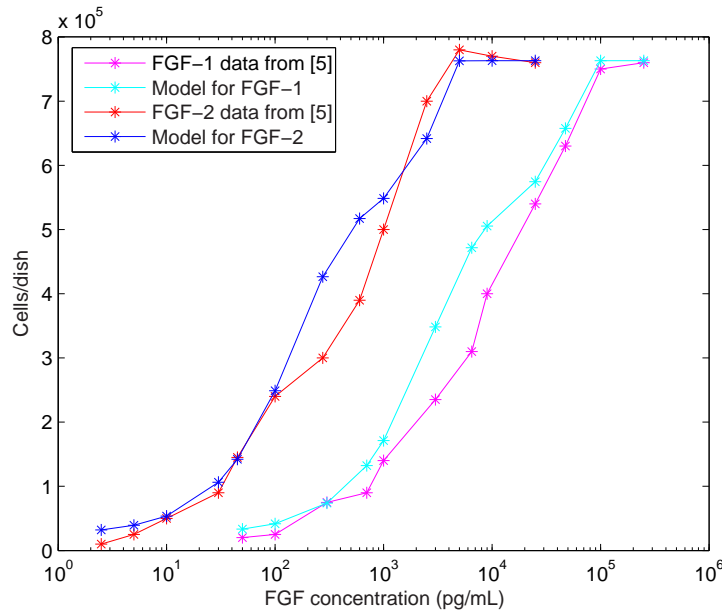
FIGURE 3. Initial Fit of Model to Biological Data from [9].

parameters μ, λ, N_0, k_4, and K_M^2:

$$\begin{bmatrix} 0.019587 & 0.775144 & 789,977 & 0.06669 & 0.011126 \end{bmatrix}.$$

The revised model, taking into account the optimal values of the parameters, is plotted along with the accompanying biological data in Figure 4.

Now we must consider the overlap between the two trials. The individual optimizations yielded slightly different values of μ, λ, and N_0, as shown in Table 5.

TABLE 5. **Comparison of Shared Parameters**

Parameter	FGF-1 trial	FGF-2 trial
μ	0.014162 h^{-1}	0.019587 h^{-1}
λ	o.468937 h^{-1}	0.775144 h^{-1}
N_0	790,568 cells	789,977 cells

Using a combined error function where the parameters are defined only once should give a compromise fit for the two trials. This combined error function yields the coefficient vector:

$$\begin{bmatrix} 0.020241 & 0.64678 & 810,667 & 1.3847 & 0.02925 & 0.077062 & 0.012556 \end{bmatrix},$$

which corresponds to parameters $\mu, \lambda, N_0, k_2, K_M^1, k_4$, and K_M^2. Figure 5 shows a plot of the model utilizing these parameters.

4.2. **Experiment 2.** Next we use MATLAB to simulate the second experiment performed by in [9]. Recall that BHK-21 cell membranes were incubated for 30 minutes in the absence of competing unlabelled FGF and in the presence of either 13 ng/mL ^{125}I-FGF-1 for part A or 14 ng/mL ^{125}I-FGF-2 for part B. To this
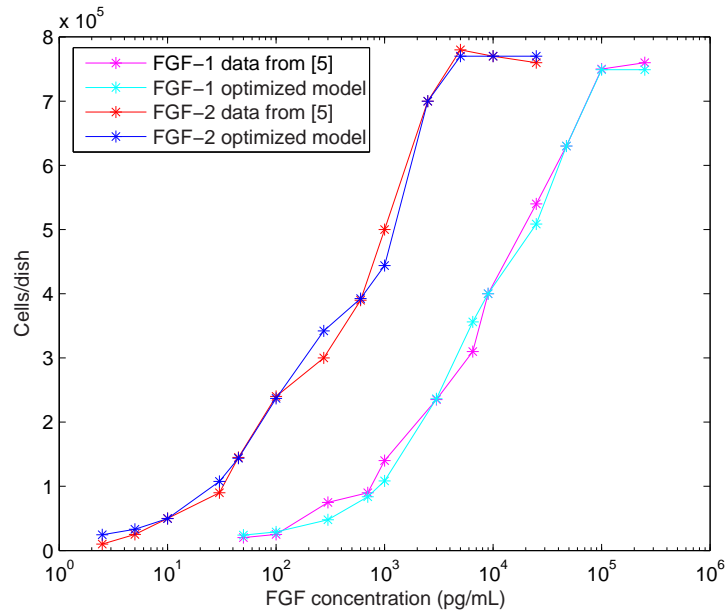
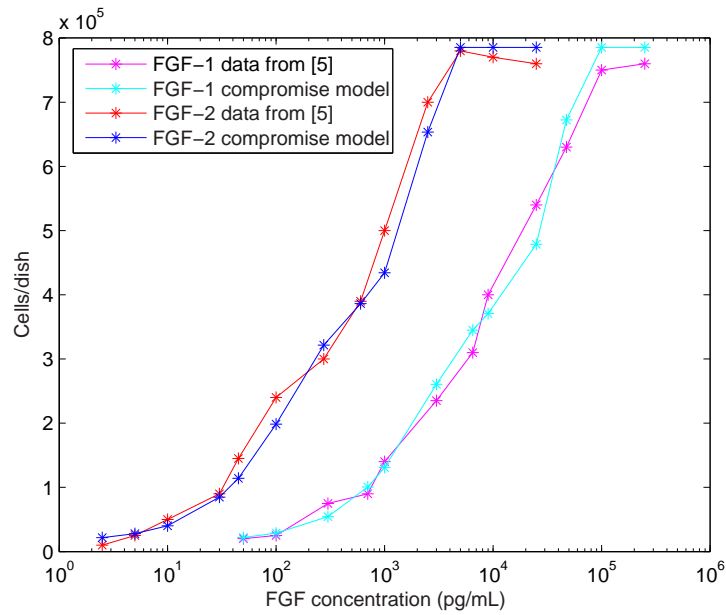FIGURE 4. Optimization Fit of Model to Biological Data from [9]

FIGURE 5. Compromise Fit of Optimization Model to Biological
Data from [9]

concentration of iodinated FGF, various concentrations of unlabelled FGF-1 and
unlabelled FGF-2 were added, as shown in Table 6.

TABLE 6. **Concentrations of FGF-1 and FGF-2 Added in Parts A and B of Experiment 2**

Part (A)		Part (B)	
FGF-1	**FGF-2**	**FGF-1**	**FGF-2**
0 ng/mL	0 ng/mL	0 ng/mL	0 ng/mL
0.5 ng/mL	0.5 ng/mL	3 ng/mL	1 ng/mL
1 ng/mL	1 ng/mL	8 ng/mL	3 ng/mL
7 ng/mL	7 ng/mL	13 ng/mL	8 ng/mL
10 ng/mL	10 ng/mL	20 ng/mL	20 ng/mL
20 ng/mL	20 ng/mL	30 ng/mL	30 ng/mL
35 ng/mL	35 ng/mL	70 ng/mL	80 ng/mL
45 ng/mL	60 ng/mL	150 ng/mL	175 ng/mL
60 ng/mL	130 ng/mL	250 ng/mL	300 ng/mL
90 ng/mL	200 ng/mL		
130 ng/mL	500 ng/mL		
180 ng/mL			
200 ng/mL			
500 ng/mL			
1000 ng/mL			

These added concentrations of growth factor along with values for the parameters K_D^1 and K_D^2, which were approximated in [9] and are displayed in Table 7, allow us to calculate the concentration of iodinated FGF for each pathway in equations (26).

TABLE 7. **Numerical Values of Additional Parameters Used in Simulations**

Parameter	Numerical Value
K_D^1	2.5 x 10^{-4} μM
K_D^2	2.7 x 10^{-4} μM

A plot showing the model for each of the pathways in parts A and B appears along with the associated biological data in Figure 6.

We now employ optimization to extrapolate the numerical values of K_D^1 and K_D^2. In order to find the optimal values of these two parameters, we again define an error function. This function is the sum of the squares of the differences of the ordinate from the biological data, p_i^{exp}, and the ordinate calculated from each pathway, p_i^{model}, as represented below:

$$E = \sum_{i=1}^{n} (p_i^{\text{exp}} - p_i^{\text{model}})^2. \tag{28}$$

Using fminsearch for this error function, the resulting coefficient vector for the parameters K_D^1 and K_D^2 is:

$$\begin{bmatrix} 3.734 \text{ x } 10^{-4} & 6.65 \text{ x } 10^{-5} \end{bmatrix}.$$

The revised model for parts (A) and (B), taking into account the optimal values of K_D^1 and K_D^2, is plotted in Figure 7 along with the associated biological data.
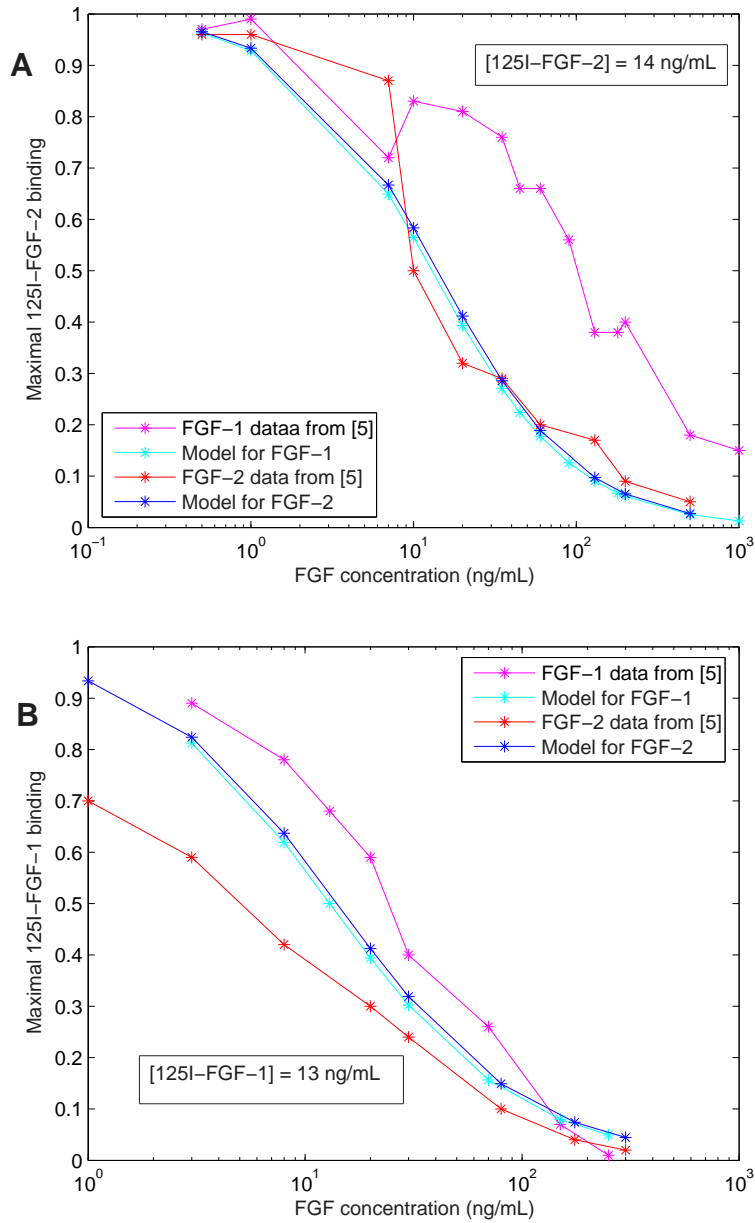
FIGURE 6. Initial Fit of ^{125}I-FGF Model to Biological Data from [9]

Using the optimized values for the parameters K_D^1 and K_D^2 along with the previously optimized values for k_2, K_M^1, k_4, and K_M^2, we can calculate the values of k_1, k_{-1}, k_3, and k_{-3}. Recall that K_M^1 is given by:
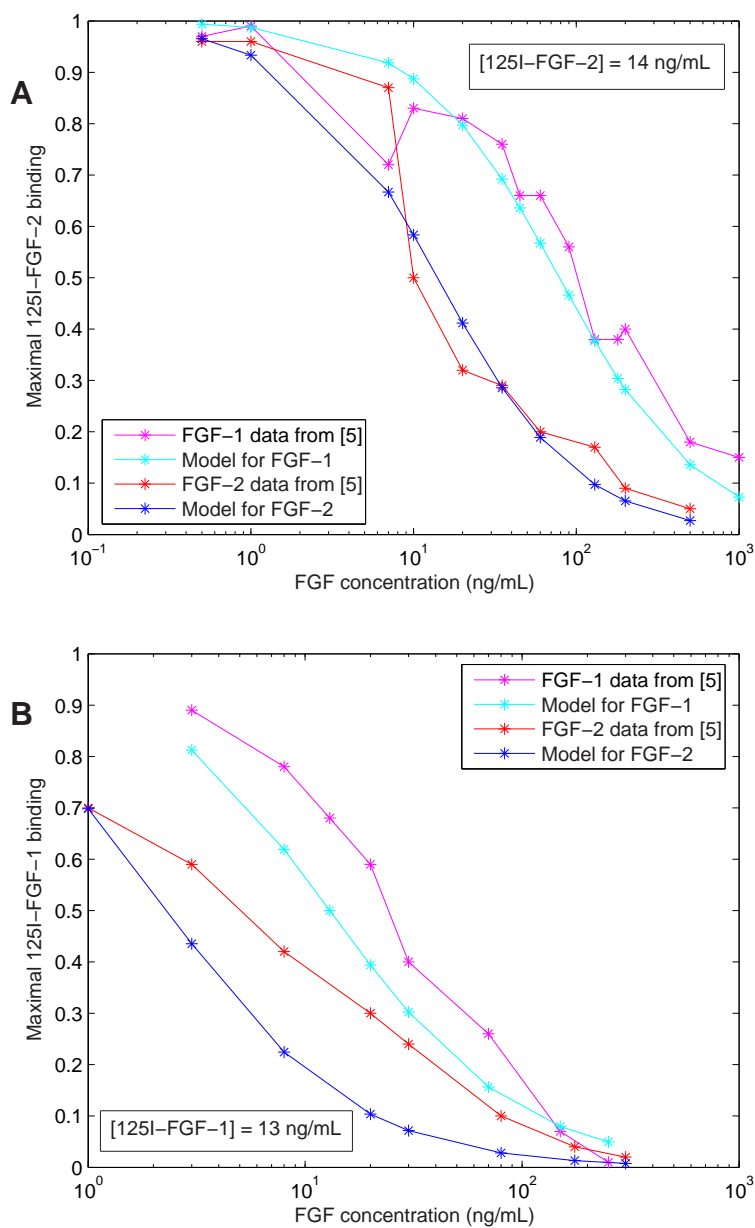
$$K_M^1 = \frac{k_{-1} + k_2}{k_1}. \tag{29}$$

FIGURE 7. Optimization Fit of ^{125}I-FGF Model to Biological Data from [9]

Using the substitution

$$K_D^1 = \frac{k_{-1}}{k_1}, \tag{30}$$

we may rewrite K_M^1 as follows:

$$K_M^1 = \frac{k_{-1} + k_2}{k_1} = \frac{k_{-1}}{k_1} + \frac{k_2}{k_1} = K_D^1 + \frac{k_2}{k_1}. \tag{31}$$

Thus, k_1 is given by:

$$k_1 = \frac{k_2}{K_M^1 - K_D^1}. \tag{32}$$

Substituting in the values of k_2, K_M^1, and K_D^1, yields a value for k_1 of 47.9507.

Moreover, we may solve the equation of K_D^1 for k_{-1} as follows:

$$k_{-1} = k_1 K_D^1. \tag{33}$$

Substituting in the values of K_D^1 and k_1 gives a value for k_{-1} of 0.0179. Likewise, we can compute the values of k_3 and k_{-3}. We find that k_3 is 6.1699 and k_{-3} is 0.00041. Table 8 displays these values along with the other optimized parameters.

TABLE 8. **Numerical Values Extracted from Optimizations**

Parameter	Numerical Value
μ	2.0241 x 10^{-2} h^{-1}
λ	6.4678 x 10^{-1} h^{-1}
N_0	810,667 cells
k_1	47.9507 $\mu M^{-1} h^{-1}$
k_{-1}	1.7905 x 10^{-2} h^{-1}
k_2	1.3847 h^{-1}
K_D^1	3.7339 x 10^{-4} μM
K_M^1	2.9250 x 10^{-2} μM
k_3	6.1699 $\mu M^{-1} h^{-1}$
k_{-3}	4.1013 x 10^{-4} h^{-1}
k_4	7.7062 x 10^{-2} h^{-1}
K_D^2	6.6474 x 10^{-5} μM
K_M^2	1.2556 x 10^{-2} μM

5. **Discussion and Future Work.** A number of findings can be drawn from our model. First, our model gives a new perspective on the relationship between K_M^i and K_D^i. Our model demonstrates that k_2 and k_4 are the driving force for experiment 1, and not K_M^1 and K_M^2 as previously thought. This result has a very important implication. It shows that k_2 and k_4 are not always insignificant, and this fact must be taken into consideration before simply disregarding the values of these parameters. Moreover, the fact that k_2 and k_4 are significant greatly affects the difference between K_M^i and K_D^i. Our results show that K_M^1 and K_M^2 are fifty to one hundred times greater than K_D^1 and K_D^2, respectively[10]. This result again has implications for future research.

---

[10]It is important to note that the values of K_D^1 and K_D^2 predicted by our model, shown in Table 8, show good agreement with the values estimated in [9] and shown in Table 7.

Second, our model demonstrates a close relationship between FGF-1 and FGF-2. By taking the ratio between the first and second equations of (14), we may write

$$\frac{d[G^1]}{d[G^2]} = \frac{\dfrac{k_2}{K_M^1}[G^1]}{\dfrac{k_4}{K_M^2}[G^2]} = \frac{k_2 K_M^2}{k_4 K_M^1}\frac{[G^1]}{[G^2]}. \tag{34}$$

Separating the variables, integrating, and exponentiating equation (34), yields

$$\frac{[G^1]}{G_0^1} = \left(\frac{[G^2]}{G_0^2}\right)^{\frac{k_2 K_M^2}{k_4 K_M^1}} \tag{35}$$

Thus, we have shown that either growth factor can be represented in terms of the other, if the initial values of both are known. This explains why the light blue and dark blue curves in the Figures 6 and 7 are parallel.

Finally, our model demonstrates the importance of parameter estimation in the modeling of biological phenomena. Slightly changing the values of parameters embedded in mathematical models can result in noticeable changes in the fit of the model. This result was shown with the optimizations we performed. Now that we have constructed our model and the parameters have been accurately estimated, we can use the model to make predictions. From our model we are able to formulate several testable hypotheses using MATLAB. We hypothesize about the appearance of several variations of experiment 1. First, we predict the outcome if the number of pulses is changed. Figure 8 shows the results of a replication of experiment 1, the only difference being that in the first trial growth factor is added only initially, the second trial follows the exact procedures of experiment 1, and the third trial entails a pulse of growth factor added initially and consecutively each of the next three days. Each of these trials still involved counting cell number at four days, and the same total amount of growth factor was added for all three. Only the average pulse size was varied for each trial.

Next, we predict the outcome of changing the number of days we wait before counting. Figure 9 compares the start of counting on day 4 instead day 6, when pulses are added initially, day 1, day 2, and day 3.

Here we notice that the greatest cell density occurs when counting earlier (day 4) rather than waiting to count (day 6). This could be attributable to the decay of the growth factor of the BHK-21 cells.

Next, we compare the effects of adding growth factor on consecutive or alternating days and then counting on day 6, as shown in Figure 10.

Here we observe that the model predicts that the trials will initially overlap and then diverge later in the experiment. This could be attributable to the growth factor decaying in the alternating trial, while the consecutive trial has enough growth factor to last longer.

Finally, we predict the effects of adding growth factor for an increasing number of pulses. As Figure 11 shows, successive trials attain greater cell density when growth factor is added for a greater number of days.
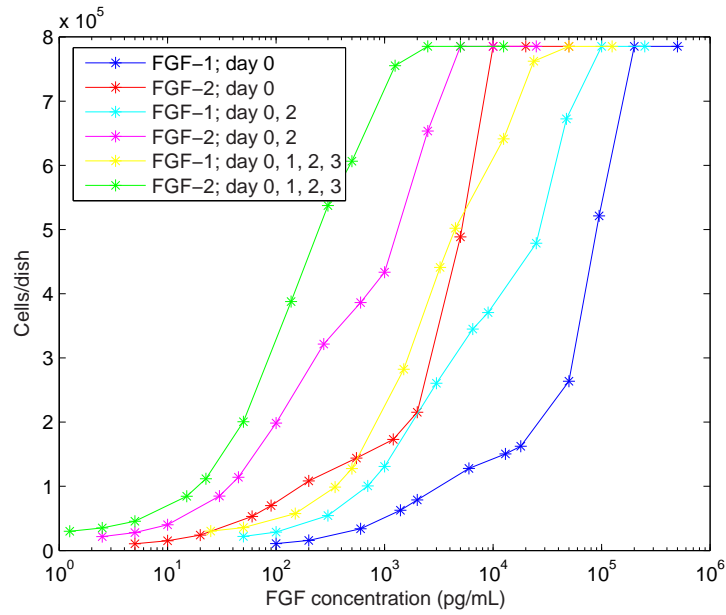
Figure 8. Simulation of Experiment 1 Showing Varying Number of Pulses (Counting Day 4)
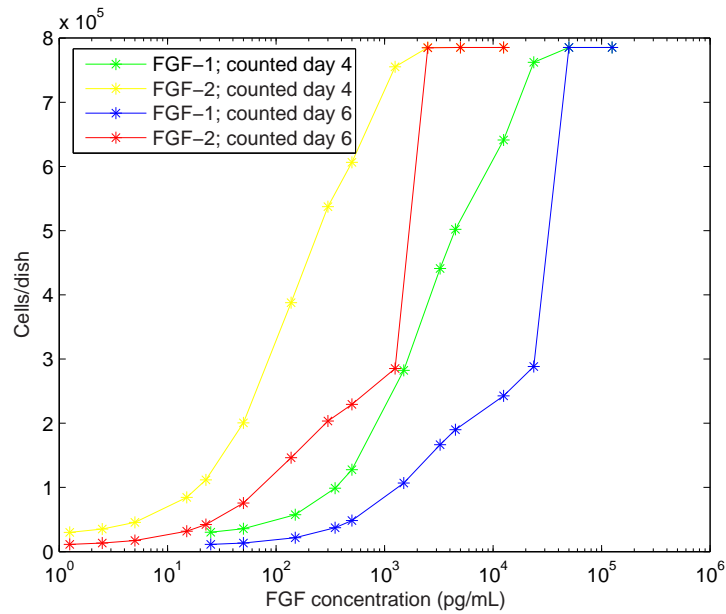

Figure 9. Simulation of Experiment 1 Showing Pulses Day 0, 1, 2, and 3 (Counting Either Day 4 or Day 6)

Here we have demonstrated that the interaction of multiple growth factors with cell surface receptors can be modeled to produce predictable outcomes. Our model
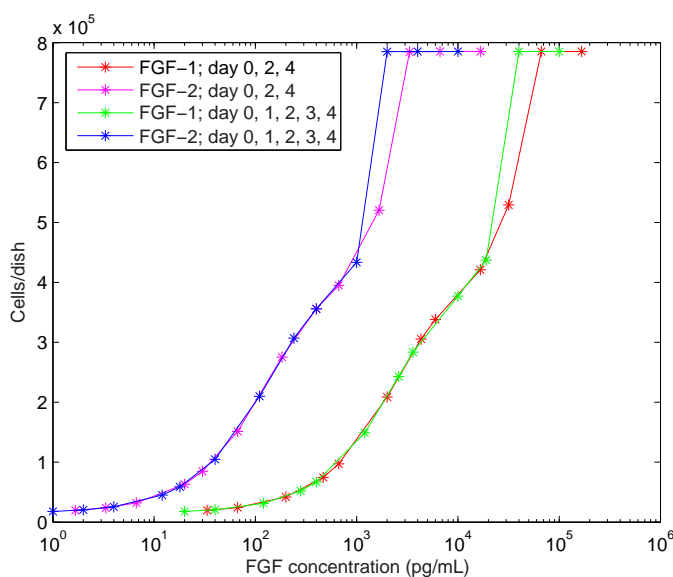
FIGURE 10. Simulation of Experiment 1 Showing Consecutive vs. Alternating Pulses (Counting Day 6)
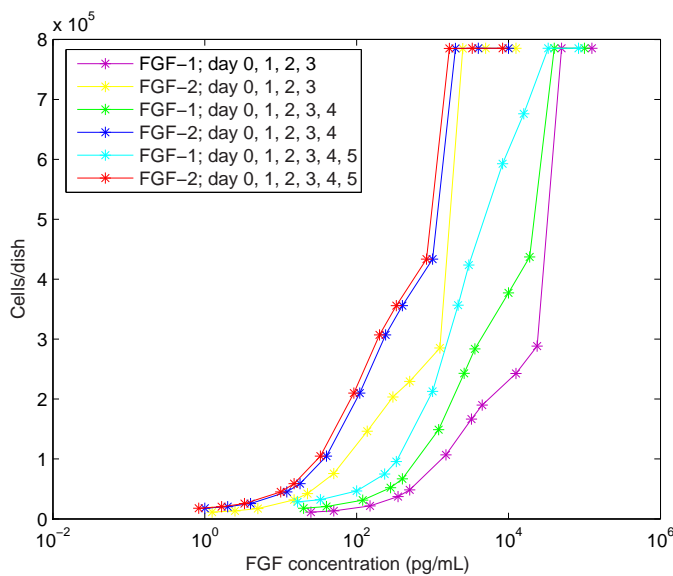

FIGURE 11. Simulation of Experiment 1 Showing Increasing Number of Pulses (Counting Day 6)

correctly describes the results of experiments performed in [9] and can predict the outcome of many experimental protocols, given accurate parameters for modelling. Although the current model was developed to simulate a relatively simple cell culture system with only two growth factors and one receptor, its capacity for

expansion to include more growth factors and growth factor receptors identifies this model as an excellent base for developing testable simulations of complex biological systems. The development of predictive models is essential to understanding the complex interplay of growth factors and their receptors, as happens during embryonic development and wound healing.

REFERENCES

[1] K. Bailey, F. Soulet, D. Leroy, F. Amalric, and G. Bouche, *Uncoupling of Cell Proliferation and Differentiation Activities of Basic Fibroblast Growth Factor*, FASEB Journal, 14, 333-344 (2000).

[2] K. Boushaba, H. A. Levine and M. Nilsen-Hamilton, *A Mathematical Model for the Regulation of Tumor Dormancy Based on Enzyme Kinetics*, Bulletin of Mathematical Biology, In Press.

[3] R.T. Bottcher and C. Niehrs, *Fibroblast Growth Factor Signaling During Early Vertebrate Development*, Endocr Rev, 26, 63-77 (2005).

[4] Y.J. Buechler, B.A. Sosnowski, K.D. Victor, Z. Parandoosh, S.J. Bussell, C. Shen, M. Ryder, and L.L. Houston, *Synthesis and Characterization of Homogeneous Chemical Conjugate Between Basic Fibroblast Growth Factor and Saporin*, European Journal of Biochemistry, 234, 706-713 (1995).

[5] L. Dailey, D. Ambrosetti, A. Mansukhani, and C. Basilico, *Mechanisms Underlying Differential Responses to Fgf Signaling*, Cytokine Growth Factor Rev, 16, 233-247 (2005).

[6] S. Ortega, M. Ittmann, S.H. Tsang, M. Ehrlich, and C. Basilico, *Neuronal Defects and Delayed Wound Healing in Mice Lacking Fibroblast Growth Factor 2*, Proc Natl Acad Sci U S A, 95, 5672-5677 (1998).

[7] M. Klagsbrun and P.A. D'Amore, *Regulators of Angiogenesis*, Annual Reviews Physiology, 53, 217-239 (1991). A.

[8] Komi-Kuramochi, M. Kawano, Y. Oda, M. Asada, M. Suzuki, J. Oki, and T. Imamura, *Expression of Fibroblast Growth Factors and Their Receptors During Full-Thickness Skin Wound Healing in Young and Aged Mice*, J Endocrinol, 186, 273-289 (2005).

[9] G. Neufeld and D. Gospodarowicz, *Basic and Acidic Fibroblast Growth Factors Interact with the Same Cell Surface Receptors*, Journal of Biological Chemists, Inc., 261(12), 5631-5637 (1986).

[10] G. Neufeld, R. Mitchell, P. Ponte, and D. Gospodarowicz, *Expression of Human Basic Fibroblast Growth Factor cDNA in Baby Hampster Kindney-derived Cells Results in Autonomous Cell Growth*, Journal of Cell Biology, 106, 1385-1394 (1988).

[11] L. Niswander, S. Jeffrey, G.R. Martin, and C. Tickle, *A Positive Feedback Loop Coordinates Growth and Patterning in the Vertebrate Limb*, Nature, 371, 609-612 (1994).

[12] L.M. Sturla, G. Westwood, P.J. Selby, I.J. Lewis, and S.A. Burchill, *Induction of Cell Death by Basic Fibroblast Growth Factor in Ewing's Scarcoma*, Cancer Research, 60, 6160-6170 (2000).

[13] D. Voet and J.G. Voet, *Biochemistry, Second Edition*, New York: John Wiley & Sons, 1995.

[14] L. Wilson and M. Maden, *The Mechanisms of Dorsoventral Patterning in the Vertebrate Neural Tube*, Dev Biol, 282, 1-13 (2005).

[15] A.O. Wilkie, Bad Bones, Absent Smell, *Selfish Testes: The Pleiotropic Consequences of Human Fgf Receptor Mutations*, Cytokine Growth Factor Rev, 16, 187-203 (2005).

E-mail address: boushaba@iastate.edu
E-mail address: marit@iastate.edu